Nanoscale

Accepted Manuscript

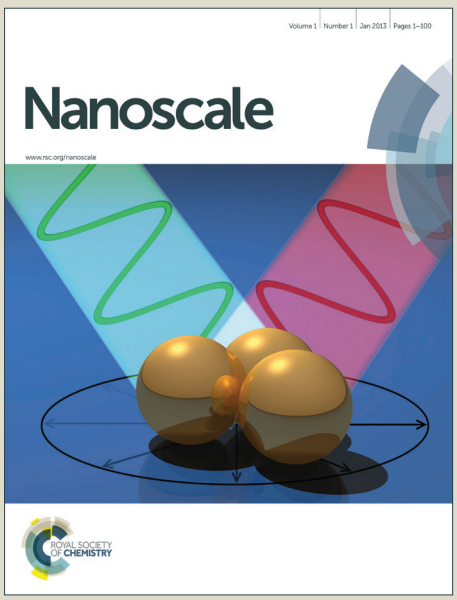

ROYAL SOCIETY OF CHEMISTRY

www.rsc.org/nanoscale

Topological Insulators based on 2D Shape-persistent Organic Ligand Complexes

Qionghua Zhou[1], Jinlan Wang[1*], Tsz Sian Chwee[2], Gang Wu[2], Xiaobai Wang[3], Qun Ye[3], Jianwei Xu[3,4], Shuo-Wang Yang[2†]

Corresponding: *jlwang@seu.edu.cn and †yangsw@ihpc.a-star.edu.sg

[1] Department of Physics, Southeast University, Nanjing 211189, P. R. China

[2] Institute of High Performance Computing (IHPC), Agency for Science, Technology and Research (A*STAR), 1 Fusionopolis Way, #16-16 Connexis, Singapore 138632, Republic of Singapore

[3] Institute of Materials Research and Engineering (IMRE), Agency for Science, Technology and Research (A*STAR), 3 Research Link, Singapore 11760, Republic of Singapore

[4] Department of Chemistry, National University of Singapore, 3 Science Drive 3, Singapore 117543, Republic of Singapore

Abstract

Topological insulators (TIs) represent an exciting new class of materials with potential applications in spintronics and quantum computing. In this work, we present a theoretical study on a new family of two dimensional (2D) nanomaterials based on the coordination of shape persistent organic ligands (SPOLs) to heavy transition metals ions such as Pd^{2+} and Pt^{2+}. These 2D structures may be readily fabricated and are expected to be stable under normal atmospheric conditions. From first principles calculations and tight-binding model simulations carried out to characterize the bulk band structures, edge states, spin Chern numbers, and the Z_2 topological invariants, we were able to identify candidates with non-trivial topological properties that may serve as topological insulators in real world applications.

Key words: 2D material, shape-persistent organic structure, topological insulator, and coordination complex

Introduction

Topological insulators (TIs), like ordinary insulators, are materials that have a bulk energy gap separating the highest occupied and lowest unoccupied electronic bands. However, they have the important distinction of hosting non-gapped states on the edges/surfaces that cross the bulk band gap, which facilitates electron conduction on the boundaries of the material.[1-3] In two dimensional (2D) TIs, spin-orbit coupling (SOC) plays a role analogous to the external magnetic field in Quantum Hall systems. The edge states are spin-polarized, and electrons with different spin orientations propagate in opposite directions.[4-5]

To date, the majority of known TIs are based on inorganic materials.[1-3,6-10] For example, quasi-2D inorganic crystals of Bi_2Te_3 and Bi_2Se_3 with superior thermoelectric properties to the bulk may be obtained by mechanical exfoliation but reproducibility remains an issue.[11] More recently, inorganic binary/ternary nanoplates and nanowires are mainly obtained via methods like chemical vapor deposition, vapor-solid or vapor-liquid-solid growth methods.[12-17] Compared to the abovementioned approaches, which are more suitable for simple binary/ternary crystalline and polycrystalline inorganic materials, traditional wet chemical synthesis is more suited for assembling complicated coordinated complexes with precise stoichiometric ratio. In both approaches, materials with high purity may be obtained.

Recently, a new type of phenyl-metal organometallic 2D structures was predicted by density functional theory (DFT) calculations to possess non-trivial topological properties.[18-20] Also, a π-conjugated nickel bis(dithiolene) ($Ni_3C_{12}S_{12}$) nanosheet was successfully synthesized[21] and later found by theoretical calculations to exhibit properties consistent with a 2D TI.[22] Unlike organometallic compounds, coordination complexes are usually stable in the presence of air and moisture. An extended planar 2D coordination framework can be fashioned in a similar way by selectively matching transition metals with a preference for square planar coordination schemes to conjugated organic ligands.

In this work, we carry out first principles calculations and tight-binding (TB) model

simulations to characterize the electronic structure and wave function topology of 2D structures assembled by the coordination of shape-persistent organic ligands (SPOLs), i.e. amino-, hydroxyl- and thio-substituted triphenylene to heavy transition metal ions, Palladium (Pd^{2+}) and Platinum (Pt^{2+}) ions. SPOLs are conjugated, planar aromatic linkers with excellent charge carrier mobility that are readily synthesized. In particular, their 2D networks normally exhibit Dirac bands akin to those found in graphene. We have chosen to study five different triphenylene ligands, namely, 3,7,11-triaminotriphenylene-2,6,10-trithiol (**1**); 3,7,11-triaminotriphenylene-2,6,10-triol (**2**); triphenylene-2,3,6,7,10,11-hexathiol (**3**); triphenylene-2,3,6,7,10,11-hexaamine (**4**) and triphenylene-2,3,6,7,10,11-hexaol (**5**) (Fig. 1a). All five organic ligands are expected to coordinate to the d^8 Pd^{2+} and Pt^{2+} ions (M) in a planar configuration that may be fully extended to form a 2D honeycomb framework as shown in Fig. 1b, where we have specifically used ligand **1** in our illustration. We study eight (8) *trans*-complexes formed by the various combinations of ligands, either **1** or **2** in Fig. 1a to the central metal ions. The *trans*- and *cis*-structures involving either amino- and NH coordinations are illustrated in Fig. 1c.

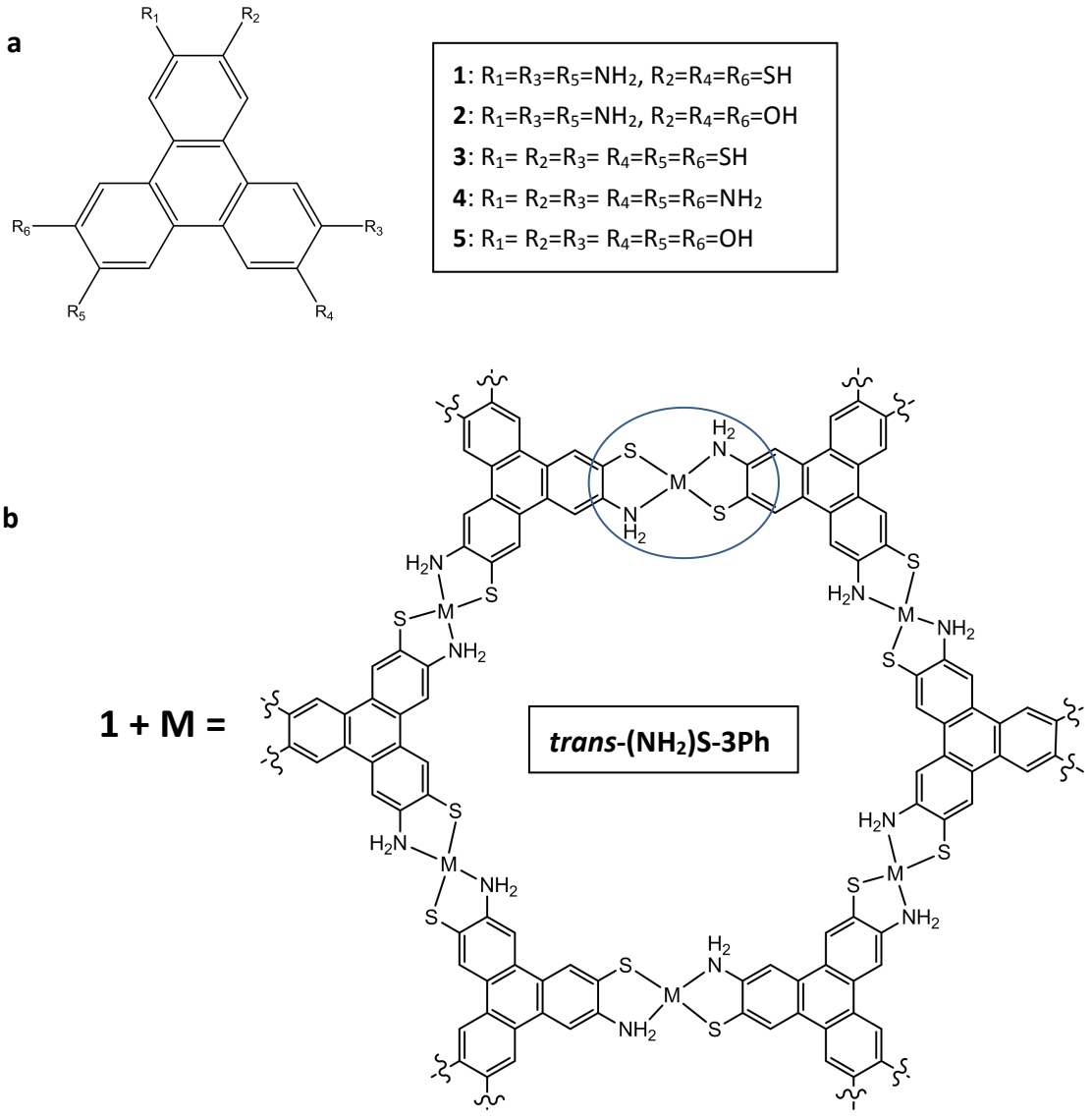

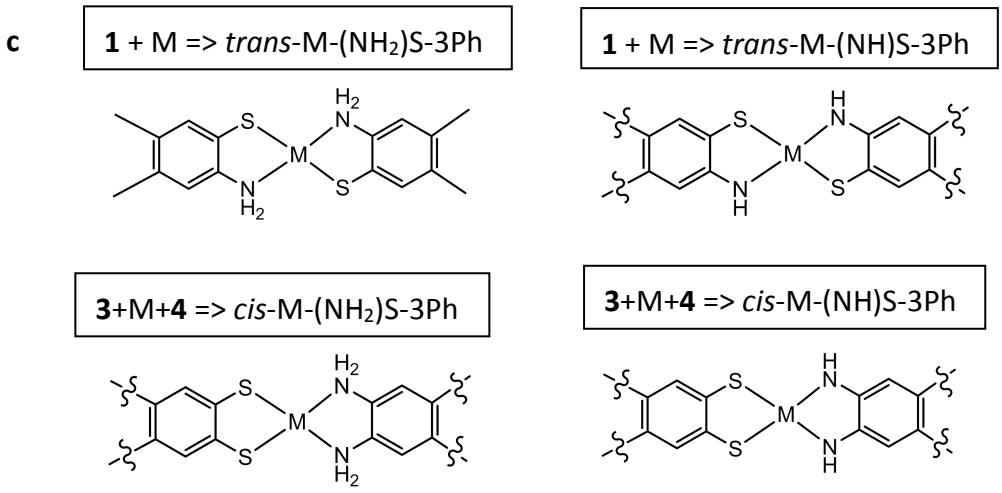

Fig. 1 (a) Five shape persistent organic ligands (SPOLs); (b) a 2D honeycomb framework formed by the reaction of **1** with M. The area enclosed by the blue solid line highlights the coordination structure of the central metal ion; and (c) two *trans*- and two *cis*-structures. When sulfur atoms are replaced with oxygen, we will have four oxo analogues.

Computational Details

First-principles calculations were carried out within the framework of density functional theory (DFT) implemented in the Vienna *ab initio* Simulation Package (VASP).[23] The exchange-correlation interactions were treated within the generalized gradient approximation (GGA) of the Perdew-Burke-Ernzerhof type.[24] The k-point meshes for self-consistent calculations are set to 5×5×1 in the Brillouin zone. Vacuum layers of 15 Å were introduced to minimize interactions between adjacent layers. All atoms were fully relaxed in each optimization cycle until atomic forces on each atom were smaller than 0.01 eV/Å and the energy variation between subsequent iterations fell below 10^{-6} eV.

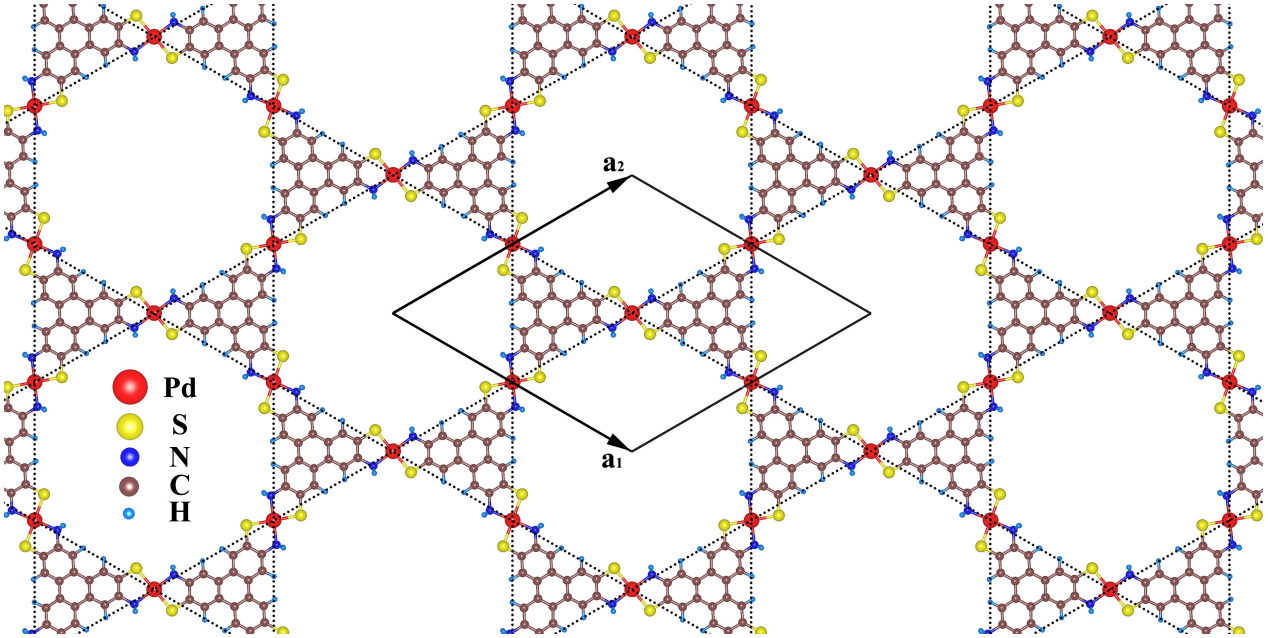

Fig. 2 The top view of 2D *trans*-Pd-(NH_2)S lattice. A unit cell is enclosed by the solid lines while the dashed lines outline the kagome lattice. The optimized lattice constant is 23.15 Å.

For ligands **1** and **2**, there are two coordination styles with either amino (NH_2) or NH to metal ions (Pd^{2+} or Pt^{2+}) to form planar 2D complexes. The former is classic amino coordination style like Cisplatin, *cis*-diamindichloroplatinum(II), a widely used cancer chemotherapeutic drug[25,26]. The 2D *trans*-Pd-(NH_2)S presented in Fig. 2 is that of the amino coordinated structures in which one of the H atoms bonded to N is hidden from the plan view. The NH coordinated complexes show diradical characteristics much like square planar bis(benzene-1,2-dithiolato) metal complexes[27,28]. Normally, diradical configurations are less stable and more reactive compared to their closed shell counterparts, which can be verified based on calculated formation energies (Table 1). But in real synthesis works, the diradical *trans*-configurations are frequently obtained.[28] A possible reason could be that, in a *trans*-diradical electronic configuration, the two unpaired electrons are delocalized throughout the 2D structure (conjugation with SPOLs), which stabilizes the whole 2D system. It is likely that reaction kinetics will also play a key role in determining the final configurations obtained, either that of the NH_2 or NH coordinated complex. In our study, we are considering both possibilities.

Results and Discussion

I. Band structures and characterization of wave function topology

Fig. 2 presents the top view of an optimized structure of the 2D *trans*-Pd-(NH_2)S lattice, where the NH_2 and S groups are coordinated to the central Pd^{2+} ion in a *trans*-like fashion with preserved space inversion symmetry. Apart from the two H atoms linked to each amino group, all other atoms reside exactly in plane. Meanwhile, each of the organic linkers **1** coordinates to three Pd^{2+} ions, resulting in a kagome lattice with six-fold symmetry. Fig. 3 illustrates the effect of incorporating SOC within our DFT calculations for mapping the energy dispersion for the three highest valence bands (kagome bands), comprising one flat band lying above two Dirac bands. The bands are spin degenerated which conform to the diamagnetic nature of square planar complexes with a d^8 electron configuration. When SOCs are included, induced gap openings in momentum space are observed at the Dirac K point ($\Delta_1 = 1.27$ meV) and Γ point ($\Delta_2 = 2.34$ meV), respectively. These gap openings are mainly due to intrinsic SOC within the *d*-orbitals of Pd atoms, herein, Rashba SOC effect can be excluded due to the inherent lattice inversion symmetry. It is also noted that the width of the gaps are relatively small. One of the reasons could be the existence of hybridization between the *d*-orbital of heavy metal atoms (Pd) and *p*-orbitals of light atoms (like N, S and C atoms) that dilutes the strength of SOC. Apart from *d*-orbital components shown in Fig. 3, we also find contributions from *p*-orbital components belonging to coordinated S atoms as well as π orbitals from the planar SPOLs (see Fig. S1 in Supporting Information (SI)). However, coordinated N atoms have not shown any *p*-orbital component among these topmost bands, which means the lone paired electrons in N atoms may donate into empty Pd *d*-orbitals and form solid bonds, and their energy bands should lie in deeper levels. By comparing Fig. 3 and Fig. S1, it is found that the weight of *p*-orbitals in these bands is higher than that of *d*-orbitals. These *p*-orbitals have little SOC effect, and the more *p*-orbital components included in the energy bands (i.e. significant hybridization), the weaker SOC occurred and the smaller gaps observed. While, by replacing heavier metallic atoms with stronger intrinsic SOC, for example, replacing Pd^{2+} with Pt^{2+}, the wider gap opening can be expected. We will discuss more details in Section II.

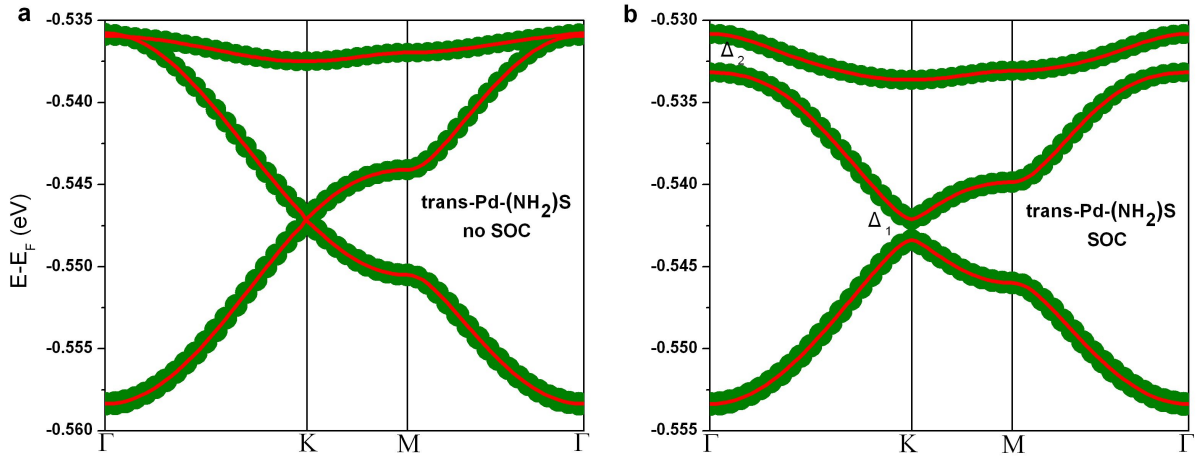

Fig. 3 The three topmost valence bands (kagome bands) of 2D *trans*-Pd-(NH_2)S lattice: (a) without and (b) incorporating SOC along the high symmetry directions. The size of the shaded circles (green) represents the relative occupancy of *d*-orbitals from Pd^{2+}. The same signs and scales are used in the following figures as well as those figures in Supporting Information (SI).

Next, we apply a single-orbital tight-binding model to this kagome lattice and reconcile this with results from our first principles calculation. Such an approach has also been taken up in previous studies.[22,29,30] The nearest and next-nearest neighbor hopping are considered in the Hamiltonian,

$$H_0 = -t_1 \sum_{\langle ij\rangle\sigma} c_{i\sigma}^{\dagger} c_{j\sigma} - t_2 \sum_{\langle\langle ij\rangle\rangle\sigma} c_{i\sigma}^{\dagger} c_{j\sigma} \qquad (1)$$

where $c_{i\sigma}^{\dagger}$ and $c_{j\sigma}$ are the creation and annihilation operators of electron with spin σ. $\langle ij\rangle$ denotes the nearest neighbor (NN) and $\langle\langle ij\rangle\rangle$ the next-nearest neighbor hopping respectively, while t_1 and t_2 are the corresponding hopping parameters. The spin-orbit term takes the form,

$$H_{SO} = i\lambda \sum_{\langle ij\rangle\alpha\beta} (\vec{d}_{ij}^{1} \times \vec{d}_{ij}^{2}) \cdot \bar{\sigma}_{\alpha\beta} c_{i\alpha}^{+} c_{j\beta} \qquad (2)$$

where λ is the SOC strength, $\vec{d}_{ij}^{1,2}$ are the unit vectors along the two nearest neighbor bonds the electron traverses going from site j to i, and $\bar{\sigma}$ is the vector of Pauli spin matrix which is reduced to s_z in our 2D situation. It can be shown that the gap opened up at the Dirac points is

equal to $2\sqrt{3}|\lambda|$, which allows us to determine that λ = 0.37 meV. The other fitting parameters are t_1 = 3.4 meV, t_2 = 0.2 meV, and E_0 = -0.54 eV, which show a good agreement with the first-principles results (Fig. 3a). However, there are still small mismatches at the Γ point mainly arising from the heterogeneous distribution of *d*-orbitals of Pd along the high symmetry directions (see shaded circles in Fig. 3).

It is known that when s_z is conserved, the spin Chern number[31] can be used to characterize 2D TIs. The Chern numbers of each kagome band with different spins are calculated using the Kubo formula[32,33] and the results are given in Fig. 4a. For these three bands, different spins result in opposite Chern numbers. $C = C_\uparrow + C_\downarrow$ turns out to be zero, which is required by time reversal symmetry. Within the SOC gaps, Δ_1 and Δ_2, the spin Chern number, defined as $C_s = \frac{1}{2}(C_\uparrow - C_\downarrow)$ was found to be 1. This further confirms that the 2D *trans*-Pd-(NH_2)S lattice, within the DFT-GGA framework, is topologically nontrivial.

In addition, we also study the edge states that impart upon 2D topological insulators their unique properties. A supercell consisting of 50 unit cells along the a_2 direction and repeated infinitely along the a_1 direction with periodic boundary conditions was used. The calculated results are given in Fig. 4b where gapless conducting states connect bulk states between both of the SOC gaps. In addition, we can see that states with different spins propagate in opposite directions due to their different group velocities. That's the well-known "spin filtered" property of 2D TIs.

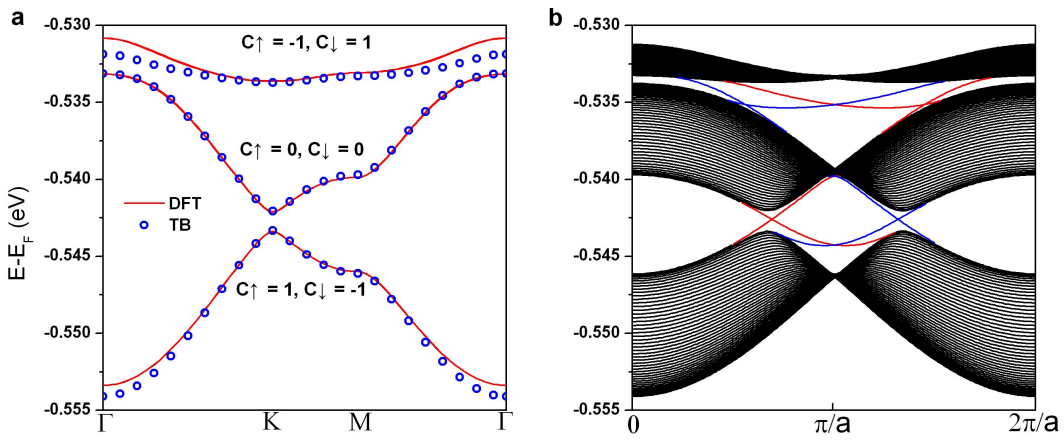

Fig. 4 (a) A comparison between DFT and TB calculated band structures for the three topmost kagome bands of *trans*-Pd-(NH_2)S. Chern numbers of each band with different spins are marked insert; and (b) edge states in the 2D *trans*-Pd-(NH_2)S lattice. Here, *a* is the lattice constant and the calculated Z_2 invariants are equal to 1. Red and blue lines denote spin-up and spin-down components, respectively. The same signs are used in the following figures as well as those figures in SI.

The Z_2 topological invariant, υ, is one of the most conclusive indicators for identifying a 2D TI even though it is complicated to determine its precise value in general. Nevertheless, Fu and Kane[34] showed that if the structure possesses space inversion symmetry, υ can be easily evaluated based on the parity of the occupied band eigenstates at the four time-reversal invariant momenta Γ_i in the 2D Brillouin zone. Accordingly, we have obtained three positive and one negative parity eigenvalues when the Fermi level is located at Δ_1. Thus, the product $\prod_i \xi(\Gamma_i) = (-1)^{\upsilon}$ gives the nontrivial υ = 1. A similar situation for electrons filled up to Δ_2 also yields υ = 1. In fact, the Z_2 invariant can also be deduced from the spin Chern number[1],

$$\upsilon = C_s \bmod 2 \qquad (3)$$

II. Substituent effects

One of the advantages afforded by a theoretical design of topological insulators based on coordination complexes is that we may systematically fine-tune their electronic structures by modifying the central metal ions and organic ligands whilst keeping their overall symmetry and network linkage intact. The replacement of Pd^{2+} with Pt^{2+} is not expected to disrupt the framework as both are d^8 ions with preferences for a square planar coordination scheme. Simple considerations of SOC suggest that the heavier Pt atom should induce a larger mixing in regions of band degeneracies leading to larger SOC-induced gaps. Our calculations on the 2D *trans*-Pt-(NH_2)S complex indicate that the three topmost valence bands also exhibit kagome-like band structures as the Pd analogue (Fig. S5). The band gaps at K and Γ points in momentum space are 2.8 meV and 5.4 meV, respectively (Table 1), expectedly larger than those found in the *trans*-Pd-(NH_2)S complex (Fig. 4).

Apart from the stronger SOC effect, we also observe higher contributions from the Pt *d*-orbitals to the kagome bands as seen in their higher occupancies. This is matched by a decrease in contributions from the *p*-orbital components from atoms (S and C) within the organic moieties (*cf.* Fig. 3 to Fig. S5). Taken together, this implies a weaker hybridization between the *d*-orbitals of Pt and *p*-orbitals of lighter atoms comparing to Pd complex, which affects the strength of SOC to a lesser extent, and results in relatively wide band gaps for *trans*-Pt-(NH_2)S. Intuitively, one expects a decrease in delocalization of the Pt *d* electrons to result in a stronger SOC since the effect is primarily mediated by the heavy metal atom. In addition, we have also fitted the DFT kagome bands to that of the TB model with a negative t_1. The sign changing of NN hopping parameter moves the flat band position from top to bottom of the Dirac bands. Further calculations on the spin Chern number, edge states (Fig. 5c & d) and the Z_2 invariant have confirmed that *trans*-Pt(NH_2)S is also topologically nontrivial with larger band gaps than the Pd analogue.

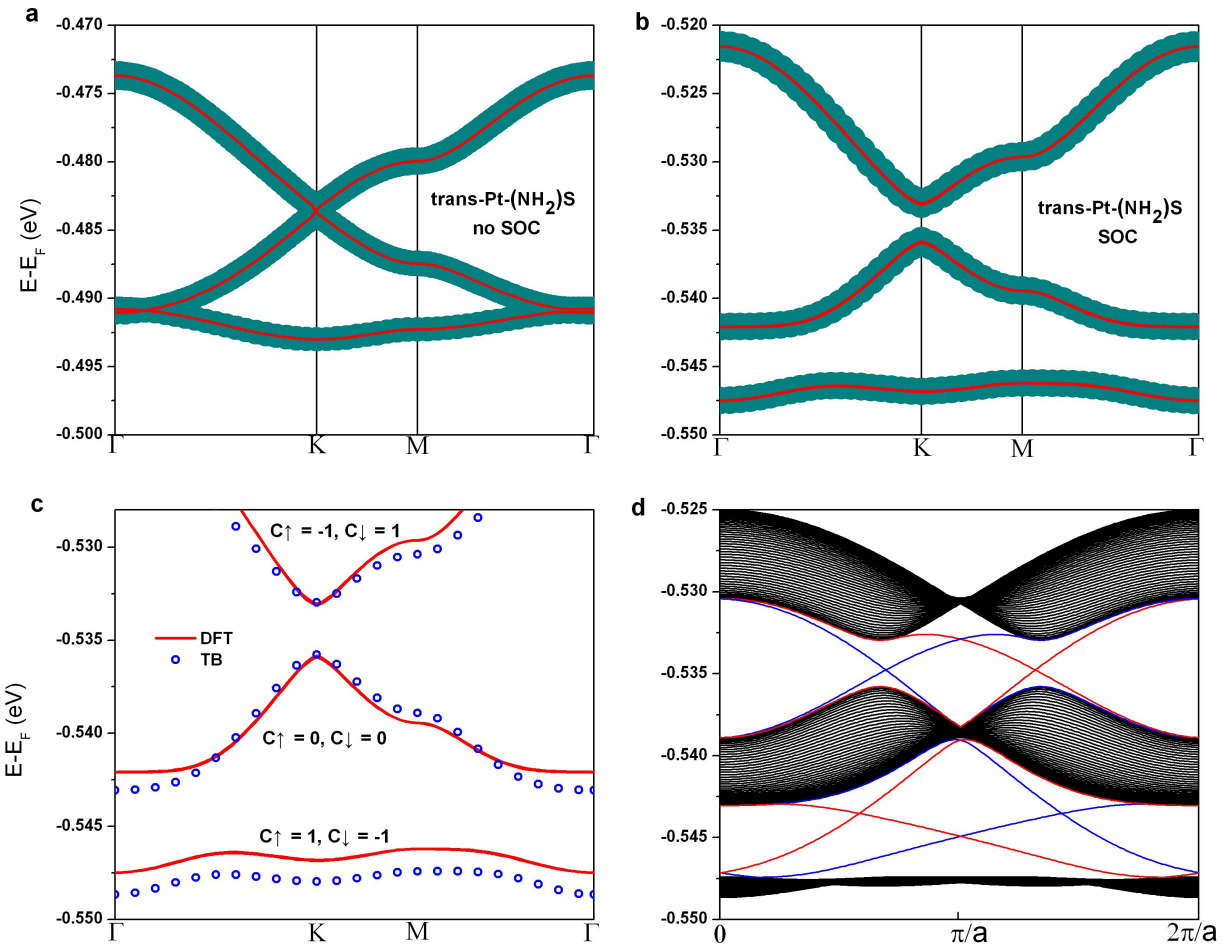

Fig. 5 (a) & (b) DFT calculated band structures of *trans*-Pt-(NH_2)S without and with SOC considerations; (c) comparison between DFT and TB calculated band structures; and (d) edge states for both up and down spins.

Table 1 DFT calculated lattice constants (a), SOC gaps (Δ_1 and Δ_2), and formation energies per unit cell (E_F^*).

Complex	a /Å	Δ_1 /meV	Δ_2 /meV	E_F/eV
trans-Pd-(NH_2)S	23.15	1.3	2.3	-10.3
trans-Pt-(NH_2)S	23.14	2.8	5.4	-15.3
trans-Pd-(NH_2)O	22.35	0.9	1.1	-6.9
trans-Pt-(NH_2)O	22.37	1.6	2.7	-11.4
trans-Pd-(NH)S	22.94	13.1	17.1	-7.2
trans-Pt-(NH)S	22.95	42.4	55.4	-13.6
trans-Pd-(NH)O	22.24	11.2	14.8	-3.4
trans-Pt-(NH)O	22.27	39.5	51.9	-9.2

*$E_F = E_{total} - 2\times E_{ligand} - 3\times E_M + n\times E_{H2}$, [n = 3 for ($NH_2$) and n = 6 for (NH)].

While our discussion so far has been centered on the *trans*-Pt/Pd complexes, we have also studied the electronic band structures of the *cis*-complexes but none of them shows non-trivial topological features. This is because they lack inversion symmetry. Besides, the lowered structural symmetry leads to poorer electron conjugation with SPOLs due to the different coordination atoms (S or N) on each side of metallic ions, and their sizes and bonding strength to the metal ions do not match well which may block/reduce the electron mobility, and subsequent relative instability as can be seen by comparing their of formation energies with the *trans*-structures (Table S1).

In addition to replacement of the central metal atom, we have also studied the effect of modifying the organic linkers on the electronic band structure. For example, sulfur may be

replaced with its congener, oxygen, while the amino NH_2 groups can dehydrogenate upon synthesis conditions and coordinate to the central metal atom to give NH. The various combinations are summarized in Table 1. In complexes where O is substituted for S such as *trans*-Pd/Pt-(NH_2)O, we also find the kagome bands to be present in their band structures (Fig. S3 & S4), even though the SOC induced gaps at both K and Γ points were found to be little bit narrow (Table 1). The diminished SOC effect may once again be rationalized by the delocalization of metal *d* electrons from the metal center such that this lessens the juxtaposition of the spin and orbital angular momentum vectors at the heavy nucleus that would have promoted SOC. Compared to S, the O atoms are smaller and chemically harder. The poorer overlap between the *p* orbitals of O and the *d* orbitals of the central metal ions results in weaker formation energies (Table 1) as well as lower *d*-orbital occupancies. As expected, the SOC gaps decrease around 0.4 ~ 2.7 meV in *trans*-Pd/Pt-(NH_2)O when compared to the sulfur analogues. Again, we did not see any *p*-orbital component from the coordinated N atoms in the three topmost bands, which indicate that the amino groups also coordinate strongly to the center metal ions in hydroxyl-coordinations.

Next, we study the NH coordinated structures which were earlier shown to have diradical character[28,35-39](Fig. 6). The sp^2 N together with bonded H atoms in these complexes lie exactly in a plane with other atoms within the molecular framework. Meanwhile, both sides of metal ions have unpaired electrons within SPOLs. The calculated lattice constants and formation energies per unit cell for *trans*-Pd/Pt-(NH)S are summarized in Table 1. Based on the DFT band structures (Fig. 7) and comparisons made between DFT and TB model calculations with inclusion of SOC effects (Fig. S5), it appears that the NH complexes are potentially better TIs since their SOC gaps (Δ_1 & Δ_2) in *trans*-Pd/Pt-(NH)S are about 7 to 15 times larger than those of their amino (NH_2) counterparts. Similar conclusions can also be drawn for *trans*-Pd/Pt-(NH)O (Fig. S6 & S7) where we again find larger SOC gaps compared to that for *trans*-Pd/Pt-(NH_2)O (Table 1).

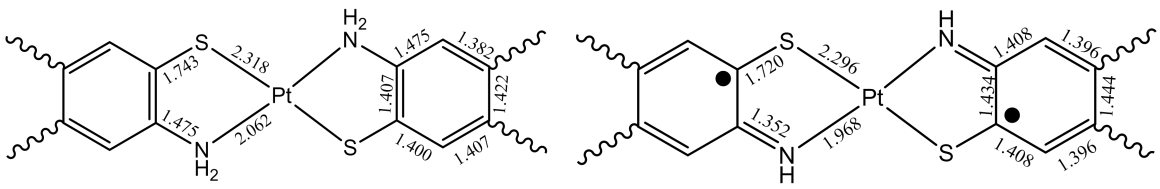

Fig. 6 The bond lengths (Å) in *trans*-Pt-(NH_2) and *trans*-Pt-(NH) complexes. The solid dots represent unpaired electrons for the structure on the right with diradical characteristics.

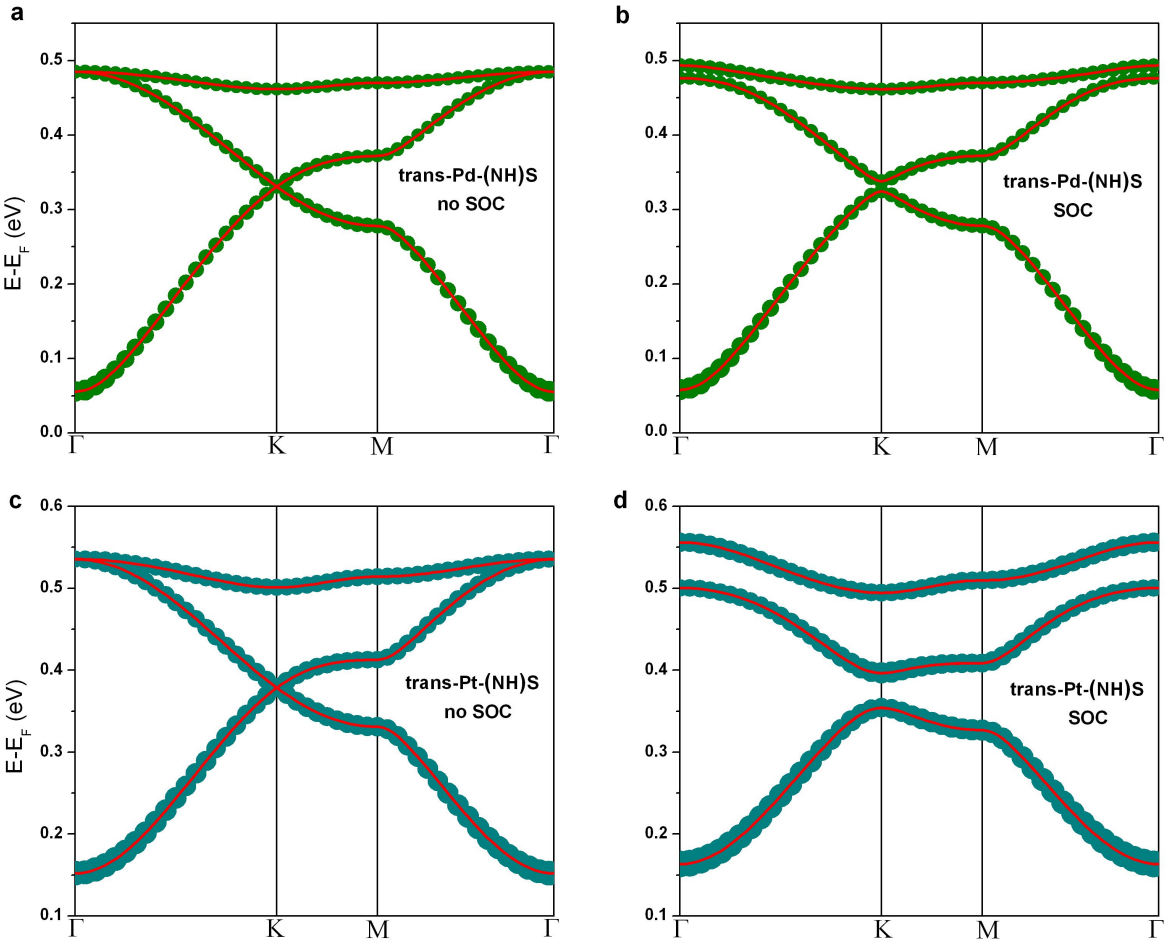

Fig. 7 (a) & (b) Band structures without and with considering the SOC effects for *trans*-Pd-(NH)S; and (c) & (d) for *trans*-Pt-(NH)S along the high symmetry directions, respectively.

To uncover the mechanism behind this, we study the orbital components in each band and compare them to that in the amino (NH_2) analogues. While the occupancies of *p*-orbitals from S, O and C atoms only differ slightly from their amino analogues (Fig. S8 & S9). While, we find additional contributions from the N *p*-orbitals within the *trans*-Pt-(NH)S/O complexes, which are not seen in complexes with NH_2 (where the N atoms are sp^3 hybridized). This N *p*-orbital component is predominantly composed of unpaired p_z electrons on the sp^2 hybridized N atoms that is similar to the p_z electrons in graphene. These lone pair electrons together with the unpaired

electrons (diradical) in the ligands are delocalized across the molecular framework and effectively extend the conjugation within the SPOLs, which stabilizes the whole 2D systems. It can be further confirmed by their calculated bond lengths in the coordination structures (Fig. 6), where the N-M bonds in NH coordinations are significantly shorter than that in amino analogues. Meanwhile, we calculate charge density differences before and after coordination reactions (Fig. S10). It is seen that electrons around nitrogen in NH_2 coordinated structures are more localized than that in NH structures. It seems that SOC in NH complexes would shrink comparing the amino complexes, which look paradoxical to our calculation results. Table 1 shows us the SOC strength in NH structure is about 7 to 25 times larger than that in NH_2 counterparts. Here, we would like mention again that t*rans*-Pt/Pd-(NH) complexes have unpaired electron cross the 2D structures which is diradical complexes. It is known, the effective SOC Hamiltonian can be written as $\xi \mathbf{L}\cdot\mathbf{S}$, where ξ is the SOC strength. $\mathbf{L}=\mathbf{r}\times\mathbf{p}$ is the angular momentum, where $\mathbf{r}$ and $\mathbf{p}$ are the position and momentum operators respectively and $\mathbf{S}$ is the spin operator. Since the angular momentum for radical or diradical systems are much larger than that of heavy metallic atoms/ions. So SOC effect in *trans*-Pt/Pd-(NH) complexes should be larger than closed shell systems[40].

We also note that the Fermi level lies outside the SOC gap at Γ point (Δ_2) for *trans*-Pt-(NH_2)S, which has a global gap of 4.1 meV between the bottom Dirac band and flat band. From a practicality viewpoint, the Fermi level should ideally be located within the global gaps. For example in *trans*-Pt-(NH_2)S, to shift the Fermi level within Δ_1, a doping of two holes per unit cell may be required due to the duplicated energy bands. For the same reason, a doping scheme of four holes is needed if the Fermi level were to migrate to within the Δ_2 gaps. The situation is slightly different for NH complexes, where each N only bonds to one H and the Fermi level drops below the kagome bands. In such a case, a doping of two electrons per unit cell may be necessary. Using the definition for doping concentration, $\rho=\frac{n}{S}$, where *S* is the surface area of the unit cell, and *n* is the number of the electrons/holes (per unit cell). We find that the doping concentration required per cell is within the range of 4×10^{13} cm^{-2} to 9×10^{13} cm^{-2}, which is experimentally accessible via electrolytic gate technology[41]. Here, also using Jellium Model to add two electrons in a cell of *trans*-Pt-(NH)S, and calculated bands (Fig. S11) clearly show the Fermi level is in

middle of SOC gap.

Conclusion

In conclusion, we have carried out first-principles calculations to characterize a new class of 2D organic topological insulators. Our calculations show spin-orbit coupling induced gap openings for all *trans*-coordinated complexes. Single-orbital tight-binding models were employed to fit the DFT band structures and calculated spin Chern number, edge states, and the Z_2 topological invariants showed that the complexes considered have non-trivial topological features. In addition, our calculations also show that the Pt complexes have larger SOC gaps compared to their Pd analogues. In addition, NH coordinations have much larger induced SOC gaps than amino counterparts. In contrast to recently reported inorganic/organometallic TIs, our proposed 2D complexes based on the coordination of shape persistent organic ligands to d^8 transition metals could be more readily synthesized. These complexes are also amendable to further functionalizations and systematic tunings to engineer larger spin-orbit gaps near the Fermi Level in the development of TIs for real world applications.

ACKNOWLEDGEMENTS

This work is supported by the NBRP (2011CB302004, 2010CB923401), NSF (21173040, 21373045) and the NSF of Jiangsu (BK20130016, BK2012322) and SRFDP (20130092110029) of China. The computation work is done using a computational facility at Department of Physics of Southeast University and National Supercomputing Center in Tianjin.

References

(1) M. Z. Hasan and C. L. Kane, *Rev. Mod. Phys.,* 2010, **82,** 3045.

(2) X. L. Qi and S. C. Zhang, *Rev. Mod. Phys.,* 2011, **83,** 1057.

(3) M. König, H. Buhmann, L. W. Molenkamp, T. L. Hughes, C. X. Liu, X. L. Qi and S. C. Zhang, *J. Phys. Soc. Jpn.,* 2008, **77,** 031007.

(4) C. L. Kane and E. J. Mele, *Phys. Rev. Lett.,* 2005, **95,** 226801; C. L. Kane and E. J. Mele, *Phys. Rev. Lett.,* 2005, **95,** 146802.

(5) B. A. Bernevig and S. C. Zhang, *Phys. Rev. Lett.,* 2006, **96,** 106802.

(6) L. Fu and C. L. Kane, *Phys. Rev. B,* 2007, **76,** 045302.

(7) B. A. Bernevig, T. L. Hughes and S. C. Zhang, *Science,* 2006, **314,** 1757.

(8) M. König, S. Wiedmann, C. Brüne, A. Roth, H. Buhmann, L. W. Molenkamp, X. L. Qi and S. C. Zhang, *Science,* 2007, **318,** 766.

(9) G. F. Wu, H. Chen, Y. Sun, X. G. Li, P. Cui, C. Franchini, J. L. Wang, X. Q. Chen and Z. Y. Zhang, *Sci. Rep.,* 2013, **3,** 1233.

(10) T. Chen, Q. Chen, K. Schouteden, W. K. Huang, X. F. Wang, Z. Li, F. Miao, X. R. Wang, Z. G. Li, B. Zhao, S. C. Li, F. Q. Song, J. L. Wang, B. G. Wang, C. V. Haesendonck and G. H. Wang, *Nat. Commun.,* 2014, **5,** 5022.

(11) P. Gehring, H. M. Benia, Y. Weng, R. Dinnebier, C. R. Ast, M. Burghard and K. Kern, *Nano Lett.,* 2013, **13,** 1179.

(12) D. Kong, W. H. Dang, J. J. Cha, H. Li, S. Meister, H. Peng, Z. F. Liu and Y. Cui, *Nano Lett.,* 2010, **10,** 2245.

(13) D. Kong, Y. L. Chen, J. J. Cha, Q. F. Zhang, J. G. Analytis, K. J. Lai, Z. K. Liu, S. S. Hong, K. J. Koski, S. K. Mo, Z. Hussain, I. R. Fisher, Z. X. Shen and Y. Cui, *Nature Nanotech.,* 2011, **6,**

705.

(14) J. J. Cha, D. Kong, S. S. Hong, J. G. Analytis, K. Lai and Y. Cui, *Nano Lett.,* 2012, **12,** 1107.

(15) S. Lee, J. In, Y. Yoo, Y. Jo, Y. C. Park, H. Kim, H. C. Koo, J. Kim, B. Kim and K. L. Wang, *Nano Lett.,* 2012, **12,** 4194.

(16) M. Safdar, Q. S. Wang, M. Mirza, Z. X. Wang, K. Xu and J. He, *Nano Lett.,* 2013, **13,** 5344.

(17) M. Safdar, Q. S. Wang, M. Mirza, Z. X. Wang and J. He, *Cryst. Growth Des.,* 2014, **14,** 2502.

(18) Z. F. Wang, Z. Liu and F. Liu, *Nat. Commun.,* 2013, **4,** 1471.

(19) Z. Liu, Z. F. Wang, J. W. Mei, Y. Wu and F. Liu, *Phys. Rev. Lett.,* 2013, **110,** 106804.

(20) Z. F. Wang, Z. Liu and F. Liu, *Phys. Rev. Lett.,* 2013, **110,** 196801.

(21) T. Kambe, R. Sakamoto, K. Hoshiko, K. Takada, M. Miyachi, J. H. Ryu, S. Sasaki, J. Kim, K. Nakazato, M. Takata and H. Nishihara, *J. Am. Chem. Soc.,* 2013, **135,** 2462.

(22) Z. F. Wang, N. Su and F. Liu, *Nano Lett.,* 2013, **13,** 2842.

(23) G. Kresse and J. Furthmüller, *Phys. Rev. B,* 1996, **54,** 11169; G. Kresse and J. Furthmüller, *Comput. Mater. Sci.,* 1996, **6,** 15.

(24) J. P. Perdew, K. Burke and M. Ernzerhof, *Phys. Rev. Lett.,* 1996, **77,** 3865.

(25) T. W. Hambley, *J. Chem. Soc., Dalton Trans.,* 2001, **19,** 2711.

(26) J. J. Wilson and S. J. Lippard, *Chem. Rev.,* 2014, **114,** 4470.

(27) K. Ray, T. Weyhermüller, F. Neese and K. Wieghardt, *Inorg. Chem.,* 2005, **44,** 5345.

(28) D. Sheberla, L. Sun, M. A. Blood-Forsythe, S. Er, C. R. Wade, C. K. Brozek, A. Aspuru-Guzik and M. Dincă, *J. Am. Chem. Soc.,* 2014, **136,** 8859.

(29) H. M. Guo and M. Franz, *Phys. Rev. B,* 2009, **80,** 113102.

(30) E. Tang, J. W. Mei and X. G. Wen, *Phys. Rev. Lett.,* 2011, **106,** 236802.

(31) D. N. Sheng, Z. Y. Weng, L. Sheng and F. D. M. Haldane, *Phys. Rev. Lett.,* 2006, **97,** 036808.

(32) Y. G. Yao, L. Kleinman, A. H. MacDonald, J. Sinova, T. Jungwirth, D. S. Wang, E. Wang and Q. Niu, *Phys. Rev. Lett.,* 2004, **92,** 037204.

(33) Y. G.Yao and Z. Fang, *Phys. Rev. Lett.,* 2005, **95,** 156601.

(34) L. Fu and C. L. Kane, *Phys. Rev. B,* 2007, **76,** 045302.

(35) E. I. Stiefel, J. H. Waters, E. Billig and H. B. Gray, *J. Am. Chem. Soc.,* 1965, **87,** 3016.

(36) D. Herebian, E. Bothe, F. Neese, T. Weyhermller and K. Wieghardt, *J. Am. Chem. Soc.,* 2003, **125,** 9116.

(37) V. Bachler, G. Olbrich, F. Neese and K. Wieghardt, *Inorg. Chem.,* 2002*,* **41,** 4179.

(38) H. Fukui, Y. Shigeta and M. Nakano, *J. Phys. Chem. A,* 2011, **115,** 1117.

(39) R. Eisenberg and H. B. Gray, *Inorg. Chem.,* 2011, **50,** 9741.

(40) I. V. Khudyakov, Y. A. Serebrennikov and N. J. Turro, *Chem. Rev.,* 1993, **93,** 537.

(41) D. K. Efetov and P. Kim, *Phys. Rev. Lett.,* 2010, **105,** 256805.